Results in Physics 3 (2013) 61–69

Contents lists available at SciVerse ScienceDirect

Results in Physics

journal homepage: www.journals.elsevier.com/results-in-physics

New approach for the spin effect on the ground state properties of the cubic and hexagonal $YFeO_3$ perovskite oxide: *GGA+U* based on the *DFT+U* description

M. Derras [a,*], N. Hamdad [b]

[a] University Djillali Liabes, Elaboration & Characterization of Materials Laboratory, Mechanical Engineering Department, Faculty of Technology, Sidi Bel Abbes 22000, Algeria
[b] University Djillali Liabès, Condensed Matter and Sustainable Development Laboratory, Physics Department, Faculty of Sciences, Sidi Bel Abbes 22000, Algeria

ARTICLE INFO

Article history:
Received 15 December 2012
Accepted 23 April 2013
Available online 3 May 2013

Keywords:
Perovskite $AFeO_3$ oxide
Spin effect
Magnetic moment
GGA+U approach
DFT+U description
U-Hubbard Hamiltonian

ABSTRACT

First-principles calculations, by means of the full-potential linearized augmented plane wave method using LSDA+U and GGA+U approach (local spin density approximation and generalized gradient approximation with U-Hubbard corrections) within the framework of spin-polarized density functional theory DFT+U were carried out for the structural, electronic and magnetic properties of the $YFeO_3$ oxide. We have calculated the lattice parameters, bulk modulus, and the first pressure derivatives of the bulk modulus for the cubic and hexagonal structures. The calculated densities of states presented in this work identify the semi-conducting behavior. Different magnetic configurations are considered for the cubic phase (NSP, FM, A-AFM, and G-AFM). The magnetic moment is also discussed.

1. Introduction

In recent years, the perovskite oxides with ABO_3 formula have gained considerable interest due to their specific properties reviewed usually in many scientist researchers: (anti)-piezoelectricity [1], (anti)-ferroelectricity [2], (anti)-ferromagnetism [3], and recently the multiferroic behavior [4], many of them show both the ferromagnetism and the ferroelectric behavior in the same times (spontaneous electric polarization and the spontaneous magnetic polarization in each field). There, they exhibit promising advantages in electrode materials for solid oxide fuel cells [5], spintronic domains [6], heterogeneous catalysts [7,8], magneto-resistance colossal [9], and also in the high capacity computer memory [10,11], wave guides, etc. These new magnetic device applications have undergone a renaissance to the perovskite materials, especially the magnetic oxides ($AMnO_3$ or the $AFeO_3$) which possess the *d* or *f* states. The magnetic properties are important factors for better understanding of the oxide behavior, it is helpful to show the spin effect on the ground state properties of the oxide.

In the present work, we represent the $YFeO_3$ perovskite oxide with another viewpoint, in order to study the magnetic properties which can be found in both cubic and the hexagonal structure, also to give a wide comprehension about the spin effect on all the ground state properties studied for the considered oxide with predictive studies. The $YFeO_3$ perovskite oxide is well known by the orthoferrite name, it is due to the orthorhombic structure which it possesses, but many researchers have proved that this oxide adopts other structures such as the cubic *Pm-3m* or the hexagonal one (investigated in the present paper) by the transformation phases due to temperature causes. The cubic structure of the $YFeO_3$ is investigated in Calle-Vallejoet et al. work [12], within the *Pm-3m* space group, where they mentioned that the perovskites were modeled in their cubic phase (space group *Pm-3m*), metals in their most stable crystal phase (except for Mn, modeled in its bcc phase), dioxides in their rutile-like structure (*P42/mnm*), sesquioxides with the *R3c* space group, except for La_2O_3 and Y_2O_3 modeled with the *P3m1* and *Ia3* symmetries respectively, and the monoxides within the *Fm-3m* (rock salt) space group for the different perovskite oxides studied. In order to account for possible distortions due to the cooperative Jahn–Teller effect on the MO_6 octahedra in the perovskite lattice [13], the Calculated Gibbs energies of formation is given in their work by the value of −11.93 eV by DFT calculation, another work was given by Moreira et al. also noted that the $YFeO_3$ adopts the cubic structure within a value of 3.785 Å [14], different scientific researchers have confirmed that our considerable oxide

* Corresponding author. Tel.: +213 048541152.
E-mail addresses: m_derras35@yahoo.com (M. Derras), n.hamdad@yahoo.fr (N. Hamdad).

2211-3797
http://dx.doi.org/10.1016/j.rinp.2013.04.001

adopts the cubic structure. In order to understand very well the $YFeO_3$ perovskite oxide behavior, the spintronic character and especially the magnetic properties where we are very much interested in the magnetic interaction in this oxide and the spin effect causes by the *d*-states of Fe element. Different magnetic configurations that are represented here, confirmed our revelation (the *d*-states of the Fe atom are responsible for the magnetic interaction on our oxide). We noted that the hexagonal structure of the $YFeO_3$ oxide is also reported in different works [15,16], Moure et al. [17] have mentioned in their paper that the cell volume of the HS polymorph is higher than the one of the equivalent OP compounds such as $YFeO_3$. Therefore, it is possible to obtain the perovskite structure from hexagonal lattices by application of high pressures [18–21]. We give here a wide description on the structural and magnetic properties of the considerable oxide, whereas the obtained results show that the magnetic moment is higher in different cubic magnetic configurations investigated than the ferromagnetic hexagonal one, and the difference is very large, this result lets us to say that the cubic structure is more important than the hexagonal structure.

2. Model and methodology in the computational details

2.1. Models

The perovskite structure has the general stoichiometry ABX_3, where A and B are cations and X is an anion. The A and B cations

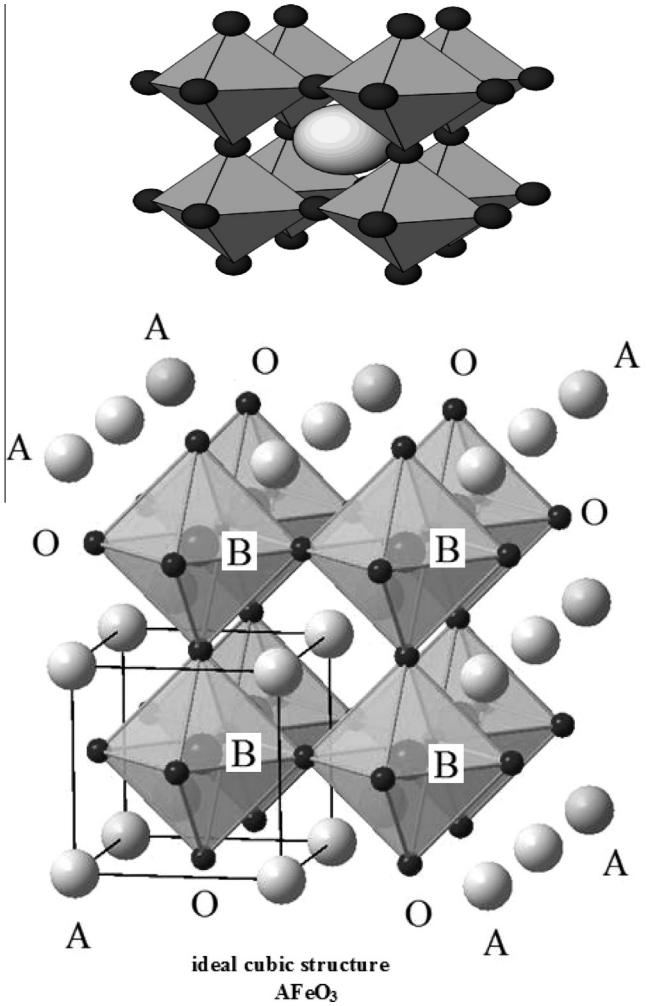

Fig. 1. The ideal $AFeO_3$ cubic crystal structure.

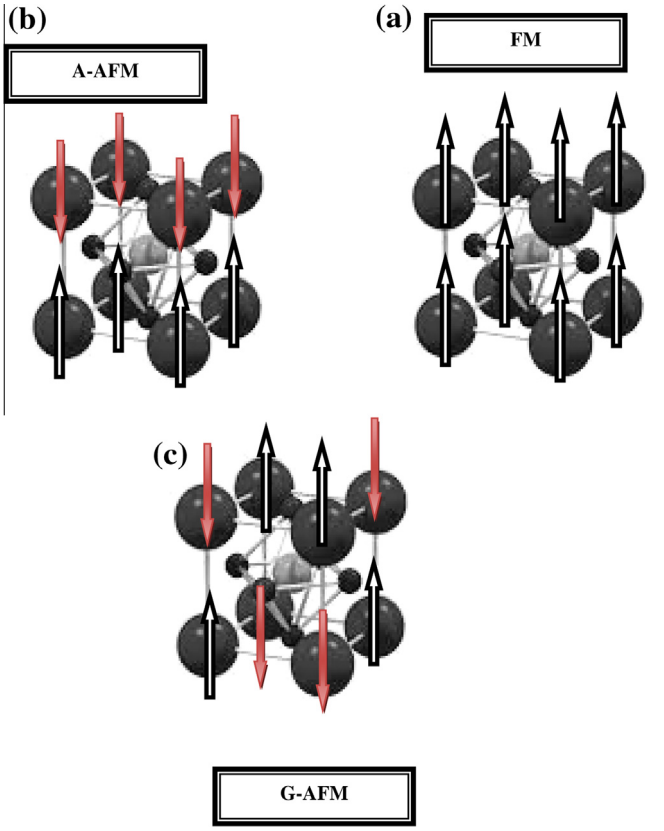

Fig. 2. Representation of the different magnetic configurations considered for our perovskite cubic oxide $YFeO_3$ (a) Ferromagnetic (*FM*), (b) Anti-Ferromagnetic *A*-type (*A-AFM*) and (c) Anti-Ferromagnetic *G*-type (*G-AFM*).

can have a variety of charges. The A cation is divalent and the B cation is tetravalent. The traditional view of the perovskite lattice is that, it consists of small B cations within oxygen octahedra, and larger A cations coordinated by oxygen. This structural family is named after the mineral $CaTiO_3$ (which was named after a Russian mineralogist, Count Lev Aleksevich von Perovski, and was discovered and named by Gustav Rose in 1839), it exhibits an orthorhombic structure with space group *Pnma* such as the $YFeO_3$ oxide [22,23]. For the $A^{3+}B^{3+}O_3$ perovskites the most symmetric structure observed is rhombohedral R3c which involves a rotation of the BO_6 octahedra with respect to the cubic structure. However, this distortion from the perfect cubic symmetry is slight. The A cations are shown at the corners of the cube, and the B cation in the center with oxygen ions in the face-centered positions. The space group for cubic perovskites is *Pm-3m* (221) (see Fig. 1). Literature suggests that many of the materials exhibit the orthorhombic *Pnma* or *Pbnm* distorted structure at room temperature. This distorted structure is shown by double the size of the cubic cell, also a further distortion is also possible which can result from a hexagonal or a rhombohedral structure with the space group *P63*cm and *R3c* respectively, the one perfect perovskite structure is described and discussed by Hines [24] to consider corner linked BO_6 octahedra with interstitial A cations. Hines suggested (solely by analysis of the tolerance factor) that the perovskite will be cubic if $0.9 < t < 1.0$, and orthorhombic if $0.75 < t < 0.9$, and whereas the value of t drops below 0.75 the compound has been seen to adopt a hexagonal ilmenite structure ($FeTiO_3$). From the literature, we noted that the considerable oxide $YFeO_3$ is well known as orthoferrite oxide [22,23,25,26], many researchers have mentioned that this material crystallized in the orthorhombic structure with the *Pnma* space group [27,28] with the lattice parameter given

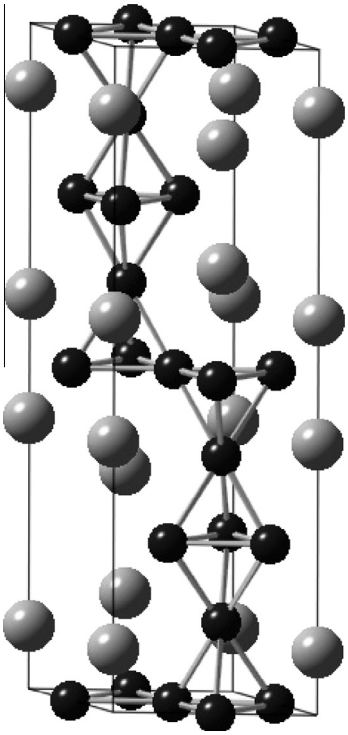

Fig. 3. The hexagonal four layered (4H) $AFeO_3$ crystal structure.

Table 1
Calculated values for the lattice parameter (*a*, *c* in Å), bulk modulus (*B*, in GPa), and its pressure derivative *B*′, for the cubic perovskite oxide $YFeO_3$ obtained using *LSDA*, *LSDA+U*, *GGA* and *GGA+U* calculations.

Material	Configuration		*a* (Å)	*c* (Å)	*B* (GPa)	*B*′
Present calculation						
$YFeO_3$		LSDA	3.6938[a]	–	241[a]	4.5[a]
	NSP	GGA	3. 7044[a]	–	233[a]	4.3[a]
	FM	GGA	3. 8214[a]	–	325[a]	6.9[a]
		LSDA+U	3. 8567[a]	–	151[a]	2.8[a]
		GGA+U	3.8619[a]	–	198[a]	4.7[a]
		GGA	3.8086[a]	3.8084[a]	116[a]	3.1[a]
	A-AFM	LSDA+U	3.9155[a]	3.9153[a]	102[a]	3.2[a]
		GGA+U	3.9209[a]	3.9206 [a]	110[a]	1.2[a]
	G-AFM	GGA	3.7365[a]	–	197[a]	3.7[a]
		LSDA+U	3.7455[a]	–	187[a]	3.4[a]
		GGA+U	3.7474[a]	–	190[a]	3.5[a]
Theoretical and experimental data						
			3.785[b]	–	–	–
			3.83[c]	–	–	–

[a] Values obtained from the present work.
[b] Ref. [49].
[c] Ref. [29].

$a = 5.2819$, $b = 5.5957$ and $c = 7.6046$ [29]. The $YFeO_3$ compound crystallized in the perovskite structure within the orthorhombic deformation, with the Neel temperature equal to 648 K. This oxide represented the anti-ferromagnetic ordering but the existence of a low ferromagnetic structure is shown, due especially to the low moments of the Fe element in the network [30], attributed to the Dzyaloshinsky-Moriya anti-symmetric exchange [31]. The Fe–O system includes three oxides, "FeO", Fe_3O_4, and Fe_2O_3. "FeO" has a cubic structure and forms a metal defect solid solution. Fe_3O_4 has an inverse spinel structure and a low solid solution range in the oxygen-rich side, and the solid solution range changes with temperature. Fe_2O has a stoichiometric composition and rhombohedral crystal system [32], a biggest technological interest is given to the phases in the Y–Fe–O system, especially of the physical specific properties which they show. As is well known, in the Y–Fe–O system, $YFeO_3$ and $Y_3Fe_5O_{12}$ are stable as ternary [33]. In the present work, we represented different magnetic configurations adopted by $YFeO_3$ in the cubic phase. We represent in Fig. 2 these configurations respectively (the ferromagnetic (*FM*), the A-type anti-ferromagnetic (*A-AFM*), and the *G*-type anti-ferromagnetic (*G-AFM*)). We noted that the space group of the (*FM*) configuration is *Pm-3m*. The *A*-type anti-ferromagnetic (*A-AFM*) and the *G*-type anti-ferromagnetic (G-AFM) configurations are designated by *P4/mmm* [15] this structure has been studied and mentioned that is metastable within $YAlO_3$, and the Fm-3m space groups respectively, whereas Fig. 3 represents the hexagonal four layered perovskite phase in the ABO_3 oxide with *P63/mmc*. In this structure the A site-cations are typically larger than the B-site cations and similar in size to those of O.

2.2. Methods

The calculation is performed using the Wien2K package [34]. This code consists of an implementation of hybrid full potential linear augmented plane wave besides local orbital (L/APW+*lo*) [35–37] method within the density functional theory *DFT* [38,39]. In the present study, we represent a new basis theory (*DFT+U* description) for the calculation of the ground state properties of $YFeO_3$ oxide. Very recently, many researchers have employed the *U*-Hubbard term by using the *LSDA+U* approach, when they implemented the exchange correlation potential treated within the *U*-Hubbard Hamiltonian. Here, we use in the structural properties part of the approach *LSDA+U* within *LSDA*, and GGA within *GGA+U* in order to compare them. GGA+U gives accurate results, also it solves all the problems found but using a smaller basis set size. This approach is based on the *DFT+U* description, which focused on a new factor named *U*-Hubbard Hamiltonian; this factor is added to the Density functional theory *DFT* basis. The smaller basis set size is due to the smaller basis set and faster matrix setup, APW+*lo* offers a shorter run-time, on the other hand it uses less memory

Table 2
Calculated values for the lattice parameter (*a*, *c* in Å), bulk modulus (*B*, in GPa), for the four layered hexagonal 4H $YFeO_3$ obtained with *GGA+U* calculations within two different magnetic configuration (non-spin polarized (NSP) and the ferromagnetic (FM).

Material	Configuration		Space group	*a* (Å)	*c* (Å)	*B* (GPa)	*B*′
Present calculation							
$YFeO_3$-4H	NSP	*GGA+U*	$P6_3/mmc$	3.6255[a]	11.5204[a]	197[a]	3.5[a]
	FM	*GGA+U*		3.6705[a]	11.7524[a]	182[a]	3.7[a]
Theoretical and experimental data							
			$P6_3/mmc$	3.5099[b]	11.759[b]		
				3.5145[c]	11.738[c]		
				3.5172[d]	11.738[d]		

[a] Values obtained from our calculations.
[b] Ref. [51].
[c] Ref. [52].
[d] Ref. [53].

than *LAPW*, so their effects are great for calculations with a large ratio of basic functions of atoms e.g. for open crystal structures, surfaces and molecules on surfaces [40]. Only the *GGA+U* is used to show the electronic and magnetic properties. All the approaches considered in the present work are introduced on the self-consistent calculation of an exchange correlation potential based on Slater's principle [41], which treats the muffin-tin spheres. In this case, the space is divided into two regions, near atoms all quantities of interest are expanded in spherical harmonic, whereas in the interstitial region plane waves are expanded. We have taken the values of 2.5, 1.9 and 1.6 Bohr for the Yttrium, ferrite and Oxygen respectively as the MT radii. The choice of sphere radius R_{mt} facilities the convergence of this expansion. The APW+*lo* method expands the khon–Sham orbitals inside the atomic muffin-tin (MT) spheres and plane waves in the interstitial region. The full-relativistic approximation without spin–orbit effects was employed in the calculation of the valence states, the core levels were treated fully relativistically. The basis set inside each MT sphere is split into core and valence subsets, whereas the core states are treated within the spherical part of the potential only and are assumed to have especially symmetric charge density, totally confined inside the MT spheres [42,43]. The k-point densities and plane wave Cuttoff energy are increased until convergence. The dependence of the total energy on the number of k-points in the irreducible wedge of the first Brillouin zone (BZ) has been explored within the linearized tetrahedron scheme by performing the calculation for 84 k-points of $14 \times 14 \times 14$ meshes, equivalent to 3000 k-points in the entire Brillouin zone (BZ). The wave has an expansion with R_{mt}. K_{max} equal to 7. We considered the self-consistent calculation to be converged only when the calculated total energy of the crystal is converged to less than 1mRyd in all calculations. We fit the curve using the Murnaghan equation [44,45]. We noted that the present results are obtained by the corrected exchange and correlation potential where the two factors introduced are the *U*-Hubbard term and the *J* factor. The *U*-Hubbard term is equal to 0.18 eV. The total density of states (DOS) was obtained using a modified tetrahedron method of Bloch et al. [28]. Different approximations are used [46–48], but only the GGA+U approach has increased the results.

3. Results and discussions

3.1. Structural properties

We investigated the structural properties by using the *DFT+U* description implemented on the wien2 K code. We note that the ideal cubic perovskite structure is well known, designated by the Pm-3m space group. The atomic positions for this structure are Y(0, 0, 0); Fe 1b(1/2, ½, ½), and O 3d(0, 0, ½), whereas the four-layered hexagonal structure was designated by the *P63/mmc* space group. The atoms are positioned at Y_1 (0, 0, 0), Y_2 (1/3, 2/1, ¼), Fe (1/3, 2/3, 0.6122), and O_1 (1/2, 0, 0), O_2 (−0.1807, −0.3614, ¼).

Different approximations *GGA*, *LSDA*, *LSDA+U* and the new approach *GGA+U* are used in order to compute the equilibrium parameter lattices for different magnetic configurations. We report the obtained values (lattice parameters: a and c (Å), equilibrium volume (Å^3), the bulk modulus B(GPa), and its pressure derivative B') for the non-spin polarized (*NSP*), the ferromagnetic (*FM*), the *A*-type anti-ferromagnetic (*A-AFM),* and the G-type anti-ferromagnetic (*G-AFM*) within different approaches: GGA, *LSDA+U*, and *GGA+U* in Tables 1 and 2 for the cubic and hexagonal structures respectively. From these tables, we see clearly that *GGA+U*

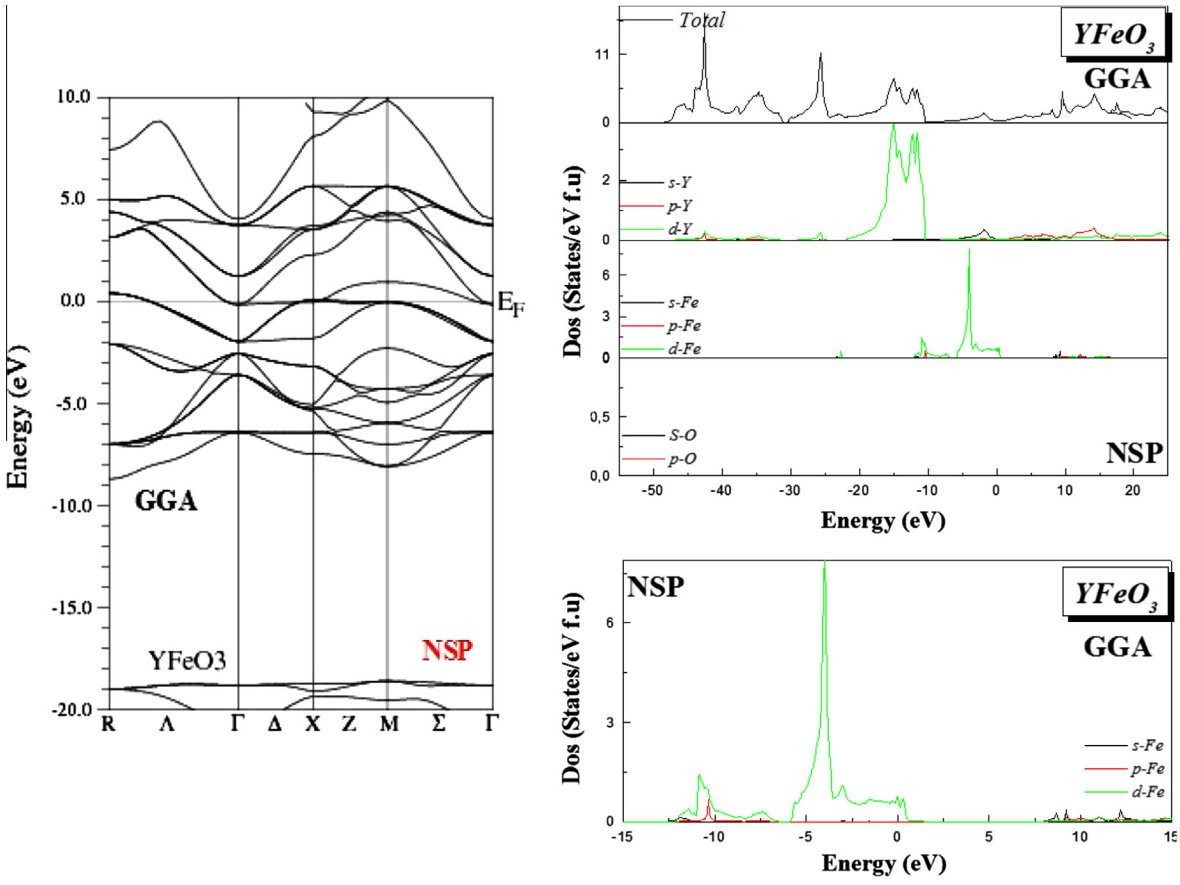

Fig. 4. The calculated *GGA* band structures and the total and partial density of states of $YFeO_3$ in the non spin polarized (*NSP*) configuration.

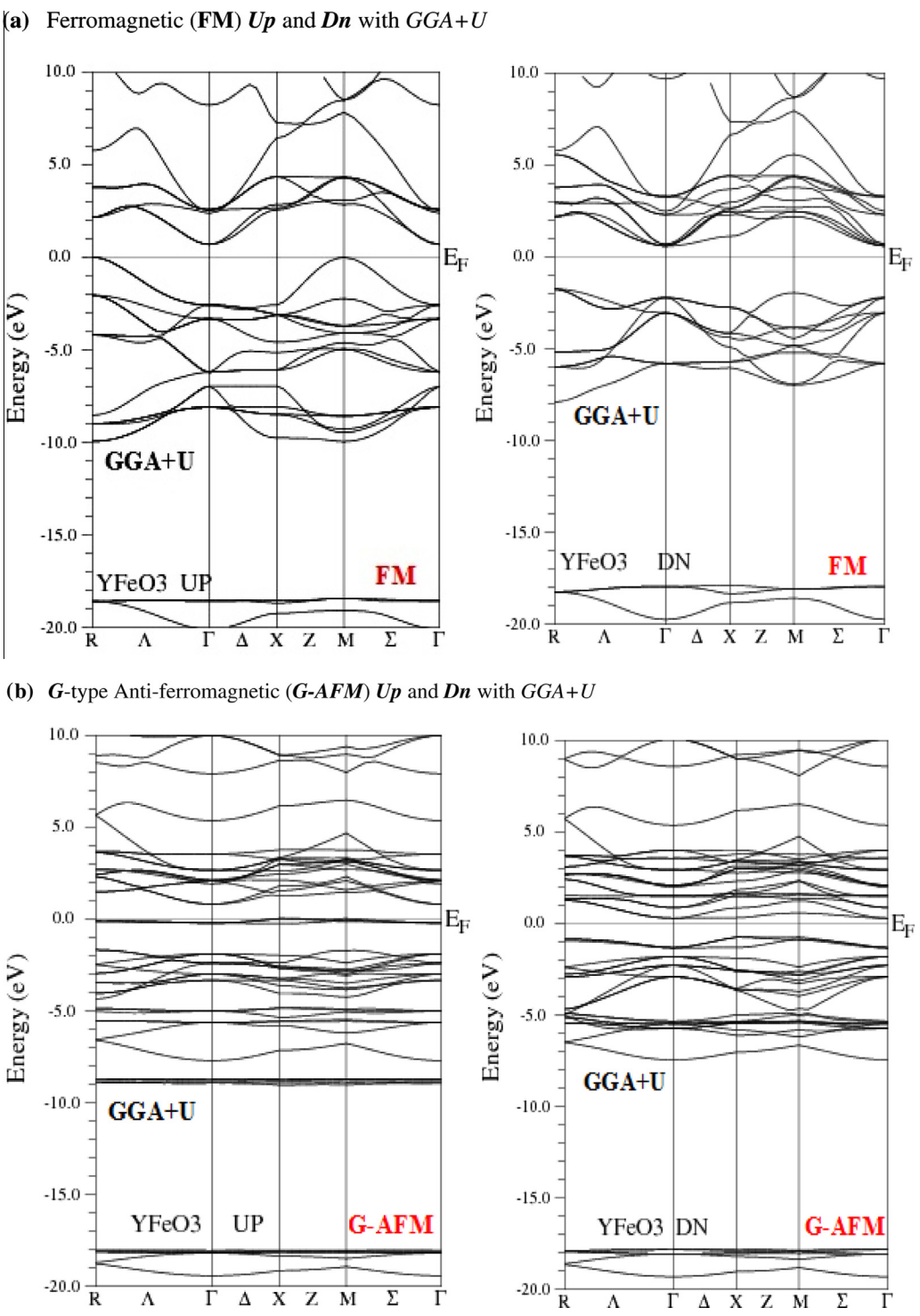

Fig. 5. The calculated *GGA+U* band structures of $YFeO_3$ in the ferromagnetic (*FM*) and the *G*-type anti-ferromagnetic (*G-AFM*) configurations respectively for $YFeO_3$. (a) Ferromagnetic (*FM*) *Up* and *Dn* with *GGA+U* and (b) *G*-type Anti-ferromagnetic (*G-AFM*) *Up* and *Dn* with *GGA+U*.

represents higher values for the lattice parameters *a* and *c* (represented in Å) than other approximations for all the magnetic configurations studied. Also it represents the under values of the bulk modulus for both structures cubic and hexagonal. Our results agree successfully with the theoretical and experimental data. We noted that the experimental parameter lattice equal to 3.83 Å, mentioned by Ray and Waghmare [29] works is near to our obtained results, they mentioned also the Stress values in (GPa) of the different magnetic configurations considered in the $YFeO_3$ oxide, where PM is equal to −15.8, FM equal to −5.9, and *AFM* equal to 2.5, where also they explained that the effects of magnetic ordering on structural instabilities are quite different (in fact, opposite sometimes) in $YFeO_3$. The value of 3.785 Å [49] approximates our obtained results 3.8214 Å, 3.8567 Å and 3.8619 Å given by the GGA, LSDA+U, and the GGA+U, respectively in the ferromagnetic configurations, as well the hexagonal results shown in our tables. Our obtained results agree very well with the experimental and the theoretical data. In the present work, we represent the $YFeO_3$

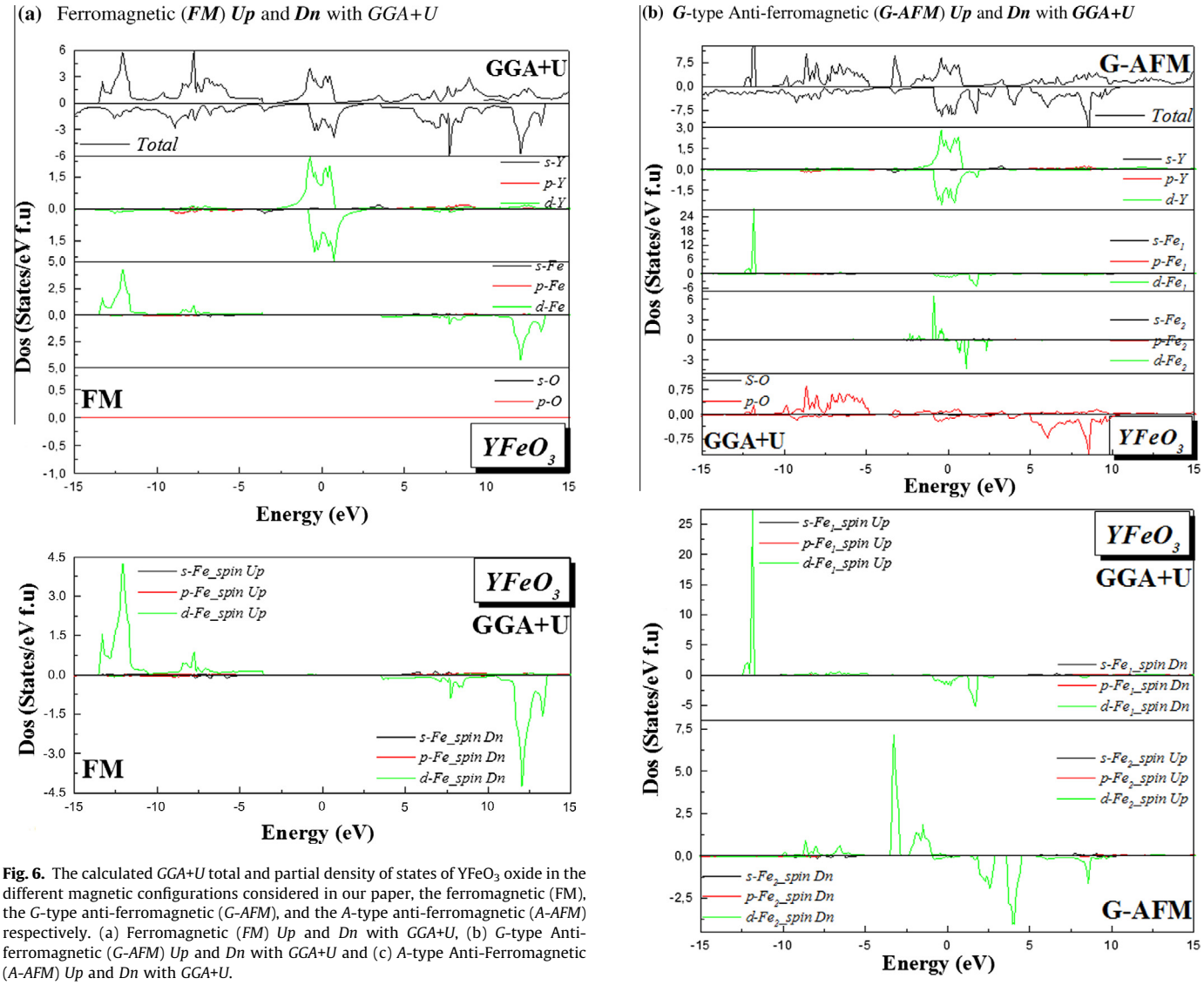

Fig. 6. The calculated *GGA+U* total and partial density of states of $YFeO_3$ oxide in the different magnetic configurations considered in our paper, the ferromagnetic (FM), the *G*-type anti-ferromagnetic (*G-AFM*), and the *A*-type anti-ferromagnetic (*A-AFM*) respectively. (a) Ferromagnetic (*FM*) *Up* and *Dn* with *GGA+U*, (b) *G*-type Anti-ferromagnetic (*G-AFM*) *Up* and *Dn* with *GGA+U* and (c) *A*-type Anti-Ferromagnetic (*A-AFM*) *Up* and *Dn* with *GGA+U*.

perovskite structure in both cubic and hexagonal structures within predictive studies in order to show the remarkable properties for our oxide. In particular, we are very much interested in the magnetic behaviour and the spin effect in different magnetic configurations investigated here. We found that the cubic structure shows more remarkable properties than the hexagonal. We remark that the *A-AFM* configuration shows higher magnetic moments than the *G-AFM,* whereas we found respectively the values equal to 4.254, and 4.149 with (Bohr Magneton), these results let us to conclude that our perovskite oxide exhibits *A-AFM* behavior.

3.2. Structural phase stability

The Yttrium orthoferrite oxide is studied by many researchers. du Boulay et al. [50] have given a detailed study on the electron density of the $YFeO_3$ oxide, using the X-ray synchrotron. He mentioned that this oxide is designated with *Pnma* for the orthorhombic structure, the map's local symmetry is influenced strongly by the Y cations, but not by neighboring O anions space group *Pnma* orthorhombic $a = 5.5877$ Å, $b = 7.5941$ Å, and $c = 5.2743$ Å at 293 K. du Boulay et al. [50] confirmed that the $YFeO_3$ oxide is essentially anti-ferromagnetic but with weak ferromagnetism as we have reported in the last paragraph but at $T_N = 644$ K, whereas the Y cation is diamagnetic. The magnetic sub-structure in $YFeO_3$ can be described by two interpenetrating pseudo-cubic face cantered sub-lattices in which each Fe cation is octahedral surrounded by six nearest neighbor anti-ferromagnetic Fe atoms. He reports that many researchers have examined the crystal structure of the considered oxide. Geller and Wood (1956) was revised by Geller (1958) and Coppens and Eibschütz (1965), analysis of possible space groups for the rare-earth orthoferrite by Marezio Remeika and Dernier (1970) strongly favors the centrosymmetric of *Pnma*, not with standing earlier attempts to refine structure using the non-centrosymmetric space group $Pbn2_1$. The magnetic sub-structure in $YFeO_3$ can be described by two interpenetrating pseudo-cubic face-centered sub- lattices in which each Fe cation is octahedral which is mentioned in the du Boulay et al. report [50].

3.3. Electronic properties

3.3.1. Band structure and density of states (DOS)

The present work using *GGA+U* treats the electronic and the magnetic properties of the $YFeO_3$ oxide. In addition, we used the population analyses to elucidate the nature of the electronic band structure, densities of states and chemical bonds. Different magnetic configurations in the cubic structure are given. The band structure and the total and partial densities of states in the non-

(c) ***A***-type Anti-Ferromagnetic (***A-AFM***) ***Up*** and ***Dn*** with *GGA+U*.

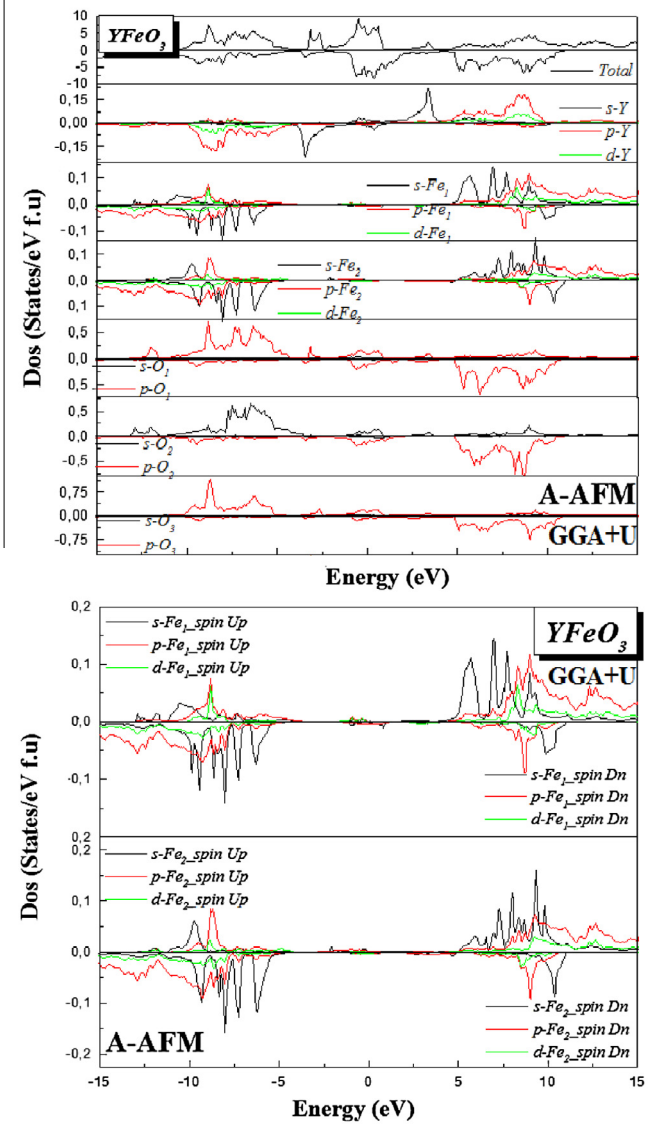

Fig. 6. (*continued*)

Table 3
Calculated magnetic moment of the $\mu_{total/cell}$, μ_Y, μ_{Fe}, and the μ_O (Bohr Magneton) of the $YFeO_3$ oxide for the ferromagnetic (FM), in the cubic structure obtained with *LSDA+U*, *GGA* and *GGA+U*.

Configuration	Approach	$\mu_{total/cell}$ (μ_B)	μ_Y	μ_{Fe}	μ_O
Ferromagnetic FM	GGA	4.037[a]	0.213[a]	3.436[a]	0.130[a]
	LSDA+U	4.997[a]	0.224[a]	4.276[a]	0.162[a]
	GGA+U	5.0 21[a]	0.226[a]	4.286[a]	0.166[a]

[a] Values obtained from our calculations.

spin polarized configuration within the *GGA* approach are shown in (Fig. 4), this figure shows the metallic behavior. We remark a negligible interaction of the oxygen element given by the *GGA* DOS figure, also a small contribution of *d*-Y states, whereas a remarkable contribution of the *d*-states of the Fe is found. Fig. 5 shows the semiconducting character for both the ferromagnetic (*FM*) and the *G*-type anti-ferromagnetic (*G-AFM*) band structure plot (within spins majorities *Up* and spins minorities *Dn*). The total and partial densities of states for the ferromagnetic (*FM*), the *G*-type anti-ferromagnetic (*G-AFM*) and the *A*-type anti-ferromagnetic (*A-AFM*) configurations of the cubic structure are shown in Fig. 6a–c, respectively using *GGA+U*. We remark from these figures, the high contribution of the *d*-states of both elements (Y and Fe), in comparison with the average contribution of their *s* and *p* states. We noted also the small contribution of the *s* and *p* states of the oxygen element in the anti-ferromagnetic configurations (*A* and *G*), this contribution does not appear in the ferromagnetic configuration figure as we see clearly. From the current figures, we remark that the *GGA+U* have show the *d*-states of the Fe atom very well, also it appears that the Fe atom contribute more than the others atoms. Both the anti-ferromagnetic configurations *A* and *G* show the semiconducting behavior. The new *DFT+U* description given in the present paper shows very well the spin states for the two electron populations (↑: for spins majorities and ↓: for spins minorities) with some differences as it appear here.

3.3.2. The magnetic moment

To gain more insight on the Fe moment formation, we calculate the local moments and the magnetic interaction in the $YFeO_3$ oxide. Here, we have considered two phases cubic (within FM, A-AFM, and G-AFM) and four-layered hexagonal (with FM configuration). We use different approaches (LSDA+U, GGA, GGA+U). Our present theoretical magnetic moment as well the experimental measurements are shown in Tables 3–6, for the (*FM*), (*A-AFM*), (*G-AFM*) configuration of the cubic structure and the (FM) of the hexagonal four layered structure. By using the moment analysis in this step of calculation, we have remarked that the magnetic moment of the Ferrite (Fe atom) is higher than others (more magnetic than both atoms the Yttrium (A atom) and the O element). From the obtained results, an important remark is revealed, we see clearly that the introduction of the *U*-Hubbard term has influenced the magnetic moment as it had influenced the structural properties. The magnetic moment is overestimated by *LSDA+U* and *GGA+U* than *GGA*. We remark also that the values obtained by *GGA+U* gives the bigger and higher values than all the approaches used. In General, the $YFeO_3$ oxide shows high magnetic properties within high values of the magnetic moment also in the cell. From these results, we concluded that a high degree of the magnetic moment values is due essentially to the presence of the (Fe) atom, in both states (spins majorities *Up*) and the states Down (spins minorities *Dn*), as well it was reported in the densities of states DOS and the band structures calculation shown here. From Table 3, we report the magnetic moment per cell values in the $YFeO_3$ oxide as following: 5.021 μ_B by *GGA+U*, it was the highest one, more than the two values of 4.037 μ_B and 4.997 μ_B, given

Table 4
Calculated magnetic moment of the $\mu_{total/cell}$, μ_Y, μ_{Fe}, and the μ_O (Bohr Magneton) of the $YFeO_3$ oxide for the *A*-type anti-ferromagnetic (A-AFM), in the cubic structure obtained with *LSDA+U*, *GGA* and *GGA+U*.

Configuration	Approach	$\mu_{total/cell}$ (μ_B)	μ_{Y1}	μ_{Fe1}	μ_{Fe2}	μ_{O1}	μ_{O2}	μ_{O3}
A-type anti-Ferromagnetic A-AFM	GGA	0·006[a]	0[a]	3.412[a]	−3.413[a]	0[a]	0.115[a]	−0.115 [a]
	LSDA+U	0.842[a]	0[a]	4.216[a]	−3.394[a]	0[a]	0.144[a]	−0.113[a]
	GGA+U	0.845[a]	0[a]	4.254[a]	−3.422[a]	0[a]	0.145[a]	−0.114[a]

[a] Values obtained from our calculations.

Table 5
Calculated magnetic moment of the $\mu_{total/cell}$, μ_Y, μ_{Fe}, and the μ_O (Bohr Magneton) of the $YFeO_3$ oxide for the G-type anti-ferromagnetic (G-AFM), in the cubic structure obtained with *LSDA+U*, *GGA* and *GGA+U*.

Configuration	Approach	$\mu_{total/cell}$ (μ_B)	μ_Y	μ_{Fe1}	μ_{Fe2}	μ_O
G-type anti-Ferromagnetic G-AFM	GGA	0[a]	0[a]	3.650[a]	−3.652[a]	0.074[a]
	LSDA+U	0[a]	0[a]	4.140[a]	−4.140[a]	0.053[a]
	GGA+U	0[a]	0[a]	4.149[a]	−4.149[a]	0.059[a]

[a] Values obtained from our calculations.

Table 6
Calculated magnetic moment of the $\mu_{total/cell}$, μ_Y, μ_{Fe}, and the μ_O (Bohr Magneton) of the $YFeO_3$ oxide for the four-layered hexagonal (4H) obtained with *LSDA+U*, *GGA* and *GGA+U*.

Configuration	Approach	$\mu_{total/cell}$ (μ_B)	μ_{Y1}	μ_{Y2}	μ_{Fe}	μ_{O1}	μ_{O2}
Ferromagnetic Hexagonal 4H	GGA	11.141[a]	0.024[a]	0.002[a]	2.384[a]	0.052[a]	0.065[a]
	GGA+U	11.144[a]	0.036[a]	0.006[a]	2.394[a]	0.058[a]	0.072[a]

[a] Values obtained from our calculations.

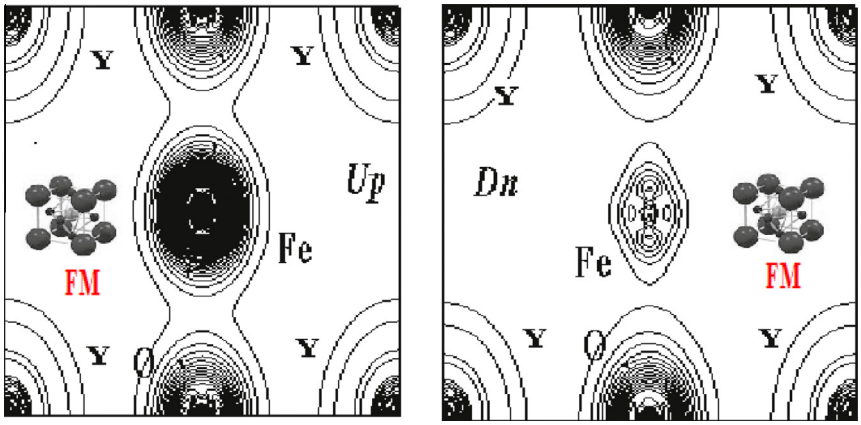

Fig. 7. The charge densities plot for the ferromagnetic configuration using the new approach *GGA+U*.

respectively by *GGA* and *LSDA+U* in the ferromagnetic configuration of the cubic phase, as well as the magnetic moment of Fe element is equal to 4.286 μ_B by *GGA+U*. The same remark is reveled in both anti-ferromagnetic configuration *A*-type and the *G*-type anti-ferromagnetic configurations, where we found the biggest values are also obtained only by *GGA+U*. We reported for *A-AFM* 4.254 μ_B and for *G-AFM* 4.149 μ_B. The same remark is also revealed in the examination of the ferromagnetic configuration (FM) of the four-layered hexagonal (4H) ferrite oxide $YFeO_3$, where we obtain the biggest values by *GGA+U* equal to 2.394 μ_B, this value is compared with the *GGA* value which is equal to 2.384 μ_B. From tables shown in this work, we remark that the magnetic moment is equal to zero in all the others atoms Y and O, or near zero, these phenomena confirm that the magnetic properties especially the local magnetic interaction are causes by the high magnetic moment of the Fe atom. The cubic phase showed more magnetic properties than the hexagonal one. From this calculation, we confirmed that the implementation of the *U*-Hubbard Hamiltonian has extensively increased the obtained results, where the localized on-site Coulomb interaction using *U* term and the exchange interaction using the *J* factor to treat the localized *d* states in the ferrite atoms plays an important role, where we give an approximate correction for the self-interaction. We noted that The U parameter defined in the PWscf is directly the $U_{eff} = U - J$ ($U = 0.18$ eV) it is used to perturb the system away from its LSDA, or GGA minimum. Finally, we concluded that *GGA+U* is more efficient.

3.3.3. Charge densities

The electronic charge density is calculated in the present paper for the ferromagnetic configuration (FM) of the cubic $YFeO_3$ oxide (see Fig. 7) using the GGA+U approach. Analysis of the Fe-orbital population's site on this configuration provides important information on the electron transfer process for the spin majorities *Up* and spin minorities *Dn*. The current analysis reveals the presence of the covalence bonding between (Fe–Fe) atoms, due essentially to the high magnetic interaction caused by the Fe element. The Fe–O bonding are covalent with a weak degree of iconicity, this nature of covalence bonding is due especially to the hybridization effect of the *d*-Fe states and the 2*p*-O states in the valence bond (VB). The Y–Y atoms show also the covalence bonding, while the ionic bonding is given between the oxygen atoms. The ionic character with a weak covalence is also found; it is due to the weak interaction between the s–Y and the 2*p*-O orbitals. Both figures for the spins majorities and the spins minorities reveal the same charge transfer between atoms with some differences, whereas the *d*-Fe states of spins Up are higher than spins Dn.

4. Discussion and summary

We studied the structural, electronic and magnetic properties of cubic and hexagonal $YFeO_3$ oxide. The exchange–correlation energy is treated by LSDA, LSDA+U, GGA, and GGA+U in the

framework of density functional theory plus U-Hubbard Hamiltonian DFT+U for different magnetic configurations. The lattice constants are found in good agreement with others works. The magnetic moment is overestimated by GGA+U. The non-spin polarized densities of states showed the metallic behavior, whereas all the others magnetic configurations considered here showed the semiconducting behavior. We concluded that the cubic phase is more important than the hexagonal phase and show more the magnetic properties. Our oxide is A-AFM.

References

[1] Fred S, Hichernell. IEEE 2005;52:737.
[2] Bednorz JG, Muller KA. Phys Rev Lett 1984;52:2289.
[3] Kabuk S, Akkus H, Mamedov AM. Physica B 2007;394:81.
[4] Mitchell RH. Perovskites. Thunder Bay, Canada: Modern and Ancient Calmaz Press; 2002.
[5] VanDoorn RHE, Bouwmeester HJM, Burgraaf AJ. Solid State Ionics 1998;111:263.
[6] Banach JG, Temmerman WM. Phys Rev B 2004;69:054427.
[7] Kim KH, Yoom KH, Choi JS. J Phys Hem Solids 1985;46:1061.
[8] Lee Jun Hee, Rabe Karin M. Phys Rev Lett PRL 2010;104:207204.
[9] Daoud-Aladine A, Martin C, Chapon LC, Hervieu M, Knight KS, Brunelli M, Radaelli PG. Phys Rev B 2007;75:104417.
[10] Piskunov S, Heifets E, Eglitis RI, Borstel G. Comput Mater Sci 2004;29:165.
[11] Auciello O, Scott JF, Ramesh R. Phys Today 1998;51(7):22.
[12] Calle-Vallejo Federico, Mart-nez José I, Garcia-Lastra Juan M, Mogensen Mogens, Rossmeisl Jan. Perovskites phases. Angew Chim. http://dx.doi.org/10.1002/anie.201002301.
[13] García-Fernández P, Aramburu JA, Barriuso MT, Moreno M. J Phys Chem Lett 2010;1:647.
[14] Moreira Roberto L, Dias Anderson. Comment on prediction of lattice constant in cubic perovskites.
[15] Li Jun, Singh Udayshankar G, Schladt Thomas D, Stalick Judith K, Scott Susannah L, Seshadri Ram. Chem Mater 2008;20:6567.
[16] Ling Wu, Yu Jimmy C, Zhang Lizhi, Wang Xinchen, Li Siukong. J Solid State Chem 2004;177:3666.
[17] Moure A, Hungrıia T, Castro A, Galy J, Peña O, Tartaj J, Moure C. Chem Mater 2010;22:2908.
[18] Ye F, Lorenz B, Huang Q, Wang YQ, Sun YY, Chu CW, Fernandez-Baca JA, Dai P, Mook HA. Phys Rev B 2007;76:060402.
[19] Huang YH, Fjellvg H, Karppinen M, Hauback BC, Yamauchi H, Goodenough JB. Chem Mater 2006;18:2130.
[20] Zhou JS, Goodenough JB, Gallardo-Amores JM, Moran E, Alario-Franco MA, Caudillo R. Phys Rev B 2006;74:014422.
[21] Lorenz B, Wang YQ, Sun YY, Chu CW. Phys Rev B 2004;70:212412.
[22] Coppons P, Eibschutz M. Determination of the crystal structure of yttrium othoferrite and refinement of gadolinium othoferrite. Acta Crystallogr 1965;19:524.
[23] Marezio M, Remeika JP, Derrier PD. The crystal chemistry of the rare-earth orthoferrites. Acta Crystallogr B Cryst Chem 1970;26:2008.
[24] Robert Ian Hines. Atomistic simulation and ab-initio studies of polar solids, Phd, Bristol, 1997.
[25] Jacob KT, Rajitha G, Dasgupta N. Ind J Eng Mat Sci 2012;19:47.
[26] Geller S, Wood EA. Acta Crystallogr 1956;9:563.
[27] Cao Xueqiang, Kim Chan-Soo, Yoo Han-Ill. J Am Ceram Soc 2001;84:1265.
[28] Kumar A, Verma AS, Bhardwaj SR. Open Appl Phys J 2008;1:11.
[29] Ray Nirat, Waghmare Umesh V. Phys Rev B 2007;77:134112.
[30] Tofield BC, Fender BEF. J Phys Chem Solids 1970;2741:31.
[31] Dzyaloshinsky J. J Phys Chem Solids 1967;241:4.
[32] Kitayama Kenzo, Sakaguchi Masanori, Takahara Youhei, Endo Hiroyuki, Ueki Hirofumi. J Solid State Chem 2004;177:1933.
[33] Kimizuka N, Katsura T. J Solid State Chem 1975;13:176.
[34] Blaha P, Schwarz K, Madsen GKH, Kvasnicka D, Luitz J. WIEN2k, an augmented plane wave plus local orbitals program for calculating crystal properties. Vienna, Austria: Vienna University of Technology; 2001.
[35] Andersen OK. Phys Rev 1975;B12:3060.
[36] Perdew JP, Wang Y. Phys Rev B 1992;45:13244.
[37] Perdew JP, Burke K, Ernzerhof M. Phys Rev Lett 1996;77:3865.
[38] Hohenberg P, Kohn W. Phys Rev B 1964;64:136.
[39] Kohn W, Sham LJ. Phys Rev A 1965;1133:140.
[40] Blöchl PE, Jepsen O, Anderson OK. Phys Rev B 1994;49:16223.
[41] Slater JC. Phys Rev 1937;51:195.
[42] Madsen GKH, Blaha P, Schwarz K, Sjostedt E, Nordstrom L. Phys Rev B 2001;64:195134.
[43] Monkhorst HJ, Pack JD. Phys Rev B 1976;13:5188.
[44] Murnaghan FD. Proc Natl Acad Sci USA 1944;30:5390.
[45] Chen Huaihui, Gauthier Paul M. Proc Am Math Soc 2011;139:583.
[46] Wimmer E, Krakauer H, Weinert M, Freeman AJ. Phys Rev 1981;B24:864.
[47] Schwarz K, Blaha P, Madsen GKH. Comput Phys Commun 2002;147:71.
[48] Sjostedt E, Nordstrom L, Singh DJ. Solid State Commun 2000;114:15.
[49] Diego M, Gil M, Carolina Navarro M, Cristina Lagarrigue J, Guimpel Raúl E, Carbonio M, Inés Gómez M. J Therm Anal Calorim 2011;103:889.
[50] du Boulay D, Maslen EN, Streltsov VA, Ishizawa N. Acta Cryst B 1995;51:921.
[51] Li Jun, Singh Udayshankar G, Schladt Thomas D, Stalick Judith K, Scott Susannah L, Seshadri Ram. Chem Mater 2008;20:6567.
[52] Croat JT, Tibbetts GG, Katz S. Science 1976;194:318.
[53] Voorhoeve RJH, Johnson Jr DW, Remeika JP, Gallagher PK. Science 1977;195:827.